






Parametric Study on Effect of Friction and Overbanding in Screening Current Stress of LBC Magnet

Jeonghwan Park , Jeseok Bang , Uijong Bong , Jaemin Kim, D. Abraimov , *Member, IEEE*, and Seungyong Hahn 

Abstract—Magnetic stress is of particular concern for ultra high field magnets, especially, peak hoop stress of those magnets may be locally concentrated by the screening current stress (SCS). For instance, the Little Big Coil (LBC), which was designed, constructed, and operated by a collaborate team led by NHMFL, generated the world record magnetic field of 45.5 T, but the conductor in LBC experienced plastic deformation due to excessive SCS. In this paper, to further analyze details of the mechanical stress behavior of LBC magnet, the effect of friction coefficient and overband radial build on stress alleviation is investigated by the parametric study. First, total current density with screening current is calculated by using the H -formulation together with domain homogenization method. Later, the entire magnet structure is modeled by the 2D finite element method to represent preload and axial interactions between each adjacent single pancake (SP), and 3 turns are assumed to be one engineering turn with frictionless radial turn-to-turn contact. While, friction acts between the coil and spacer in a direction that limits the radial displacement. Finally, we discuss the effects of friction coefficient and overband thickness by sweeping those parameters. Our parametric study implies that both friction and overband radial build can reduce peak hoop stress levels of LBC, however, effect of friction is dominant when overbanding is thicker than 0.5 mm.

Index Terms—Mechanical stress analysis, no-insulation, parameter sweep, screening current stress.

I. INTRODUCTION

OWING to the in-field high critical current density, excellent mechanical robustness, high stability, and excellent protection, the no-insulation (NI) technique enabled constructing ultra-high field magnets [1]–[15]. However, there is a growing concern for screening current stress (SCS) which may cause a local concentration of high magnetic stress. Precise estimation

Manuscript received December 1, 2020; revised February 23, 2021; accepted March 17, 2021. Date of publication March 31, 2021; date of current version May 14, 2021. This work was supported by Samsung Research Funding & Incubation Center of Samsung Electronics under Project SRFC-IT1801-09. (Corresponding author: Seungyong Hahn.)

Jeonghwan Park, Jeseok Bang, Uijong Bong, Jaemin Kim, and Seungyong Hahn are with the Department of Electrical and Computer Engineering, Seoul National University, Gwanak-gu, Seoul 08826, South Korea (e-mail: hahnscy@snu.ac.kr).

D. Abraimov is with National High Field Magnet Laboratory, Florida State University, Tallahassee, FL 32319 USA.

Color versions of one or more figures in this article are available at <https://doi.org/10.1109/TASC.2021.3070097>.

Digital Object Identifier 10.1109/TASC.2021.3070097

and mitigation of SCS with consideration of radial turn-to-turn contact of NI magnets are key challenges for high field NI magnets.

The significance of SCS was firstly reported by the world record 45.5-tesla (T) direct-current magnet, called Little Big Coil (LBC), where plastic rippling deformation was discovered [1]. Later with the post-mortem analysis of LBC, a shifting of the bending center of the conductor was observed as a consequence of SCS [16]. Still, one of the remaining problems is that the coil experiences excessively high SCS which exceed the ultimate tensile strength limit of the REBCO conductor, according to our previous numerical calculation results [16]. To further analyze details for the mechanical stress behavior of LBC magnets, we investigate the effects of different construction variables, such as overbanding thickness and friction coefficient.

First, nonuniform current densities in LBC due to the screening current were calculated with the finite element analysis (FEA) adopting H -formulation. Next, mechanical stress was calculated by the FEA, where contact-pair boundary condition was adopted to consider radial turn-to-turn contact behavior of every individual turns. The entire magnet structure was modeled for consideration of preload as well as axial force interactions between adjacent single pancakes (SPs). Meanwhile, three turns were set to be one engineering turn, for which frictionless contact for radial turn-to-turn contact, but frictional one for the contact between the spacer were considered. Finally, the parameter sweep approach with respect to the friction coefficient and radial overband was applied for the mechanical analysis. The analysis results imply that both friction force and overband radial build can mitigate peak hoop stress.

II. MODELING OF NON-UNIFORM CURRENT DENSITY

A. Screening Current Calculation Method and $E - J$ Characteristics: H -Formulation and Index Model

Considering the 2D-axisymmetric of LBC, which is a solenoid magnet, FEA based simulation method adopting H -formulation is used to calculate non-uniform current densities with screening current. The governing equation for the H -formulation method, whose details are well-explained in other literature [17]–[19], is Faraday's law of induction. In this particular method, 2D-axisymmetry edge-element together with

TABLE I
KEY PARAMETERS OF LBC MAGNET

Parameters	Values
Magnet Dimension	
Inner radius, a_1 ; outer radius, a_2	[mm] 7; 17
Total height, $2b_1$	[mm] 53.1
Number of pancakes	12
Young's moduli of conductor, $E_r; E_h; E_z$	[GPa] 69; 144; 144
Poisson ratio of conductor, $\nu_{rh}; \nu_{hz}; \nu_{zr}$	0.38; 0.34; 0.20
Young's moduli of structure	[GPa] 20 (spacer); 200 (overbanding)
Poisson ratio of structure	0.3 (spacer, overbanding)
Magnet Operation	
Maximum operating current, I_{op}	[A] 245.3
Operating temperature, T_{op}	[K] 4.2
Background magnetic field	[T] 31.1

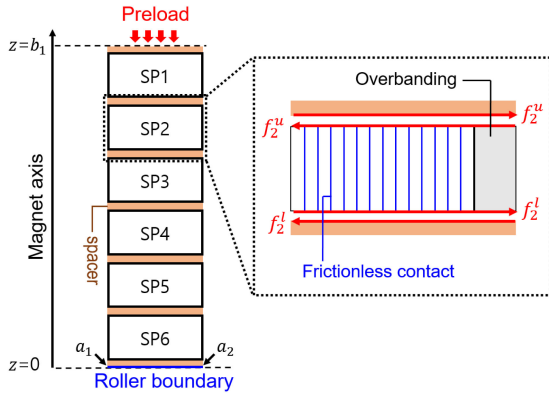


Fig. 1. Description of boundary conditions applied for mechanical modeling. A preload of 86 kg is applied at the top of the magnet, and a roller condition is given at the mid-plane. Radial turn-to-turn contacts are modeled as frictionless contact, and bulk overbanding structure is considered. The direction of the friction is against the radial displacement of each SP.

the domain homogenization technique was used to reduce the computational cost. $E - J$ characteristic of an REBCO conductor is expressed with the well-known power law, also known as the index resistance model [20]:

$$E_\phi = E_c \left| \frac{J_\phi}{J_c} \right|^n, \quad (1)$$

where E_ϕ , E_c , J_c , J_ϕ , n are, respectively, circumferential electric field, critical electric field of $1 \mu\text{V}/\text{cm}$, critical current density, current density of the winding, and index value. Due to the lack of information on measurements of critical current as well as an index value in an ultra-high field ($>40 \text{ T}$), we obtained extrapolated critical current data with the well-known practical fit function [21], and the index value was assumed as $n = 20$ [22].

B. Analysis Target: Magnet Parameter and Operating Scenario of LBC

NI REBCO high temperature superconductor (HTS) insert of LBC, which generated 14.4 T in a background of 31.1 T LTS outsert, is designed, constructed, and operated by a team NHMFL. Table I summarizes key parameters of the magnet, which consists of 6 double pancake (DP) coils with a total height of 53.1 mm as shown in Fig. 1. The coil is wound

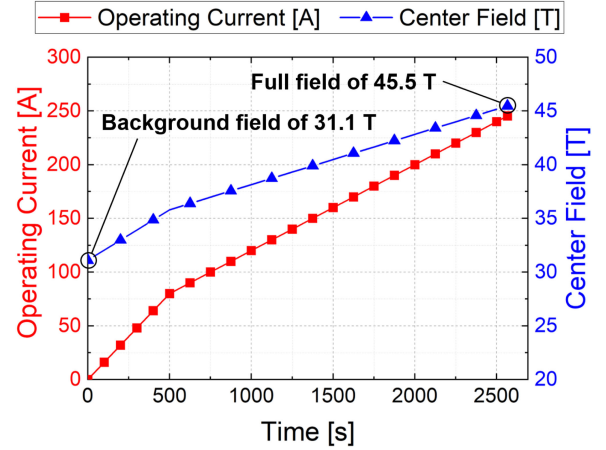


Fig. 2. Operation results of LBC magnet with operating current and measured center field. Simulation results at a full field of 45.5 T will be presented in the latter analysis.

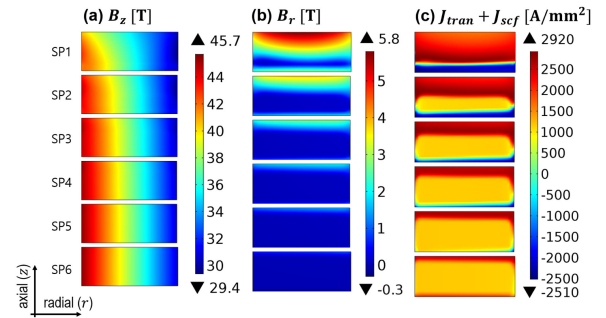


Fig. 3. 2D axisymmetric section view that represents FEA results for the upper half of the magnet: (a) axial magnetic field, B_z ; (b) radial magnetic field, B_r ; and (c) total current density (transport + screening), $J_{tran} + J_{scf}$. Maximum current density of $2920 \text{ A}/\text{mm}^2$ is calculated at SP3.

by $44 \mu\text{m}$ thick SuperPower conductor which is composed of $5 \mu\text{m}$ thick electroplated copper stabilizer, and $30 \mu\text{m}$ thick Hastelloy substrate. Correspondingly, the magnet features high engineering current density of $1020 \text{ A}/\text{mm}^2$. For the calculation of screening current distributions together with the transport current, the power supply operating scenario shown in Fig. 2 is considered. All the following simulation results are shown at the moment of the full field of 45.5 T.

C. Simulation Results of Screening Current Distributions

Fig. 3 shows screening current calculation results of LBC magnet for the upper half of the magnet: (a) axial magnetic field, B_z ; (b) radial magnetic field, B_r ; and (c) total current density (transport + screening), $J_{tran} + J_{scf}$. Essentially, more screening current is induced at the SP which experiences a larger radial magnetic field, therefore, the penetrated screening current mostly happens in SP1. While, peak current density occurs at SP3 with a value of $2920 \text{ A}/\text{mm}^2$, which is about twice larger than the conductor current density of $1420 \text{ A}/\text{mm}^2$ without the screening current.

TABLE II
 AXIAL PRESSURE OF EACH SP DUE TO LORENTZ FORCE

	SP1	SP2	SP3	SP4	SP5	SP6
Pressure [MPa]	17.5	26.1	30.9	33.5	35	35.5

III. PARAMETRIC STUDY ON SCREENING CURRENT STRESS

A. Mechanical Stress Modeling: Entire Magnet Modeling With Discrete Contact Mechanics

Fig. 1 shows a 2D-axisymmetric model for the upper half of the magnet. Governing equation for the mechanical analysis is given by

$$\vec{\nabla} \cdot \sigma + \vec{f}_v = 0, \quad (2)$$

where σ is a stress tensor, and \vec{f}_v [N/m³] is volumetric Lorentz force vector acting on the conductor. Then, the relation between stress and strain is given by the generalized Hooke's law. For the sake of consideration of axial interactions between each adjacent SP, whole SP magnets are modeled together with G10 spacers in between each SP. A preload of 86 kg, which corresponds to 1.1 MPa in pressure, is assumed to be uniformly distributed at the upper boundary of SP1. With the symmetry to the mid-plane, the roller condition is given at the lowermost spacer by:

$$\vec{u} \cdot \hat{n} = 0, \quad (3)$$

where \vec{u} and \hat{n} are displacement vector and a unit vector normal to the surface. The turn-to-turn contacts of every SP are modeled by frictionless unilateral contact, and the penalty method is adopted for the analysis [23], [24]. For the ease of computational cost, 3 turns are regarded as one engineering turn, and linear elastic properties in Table I is assumed [25].

Friction forces act in the direction of blocking the radial displacement of the individual turns as illustrated in Fig. 1 [26]. The friction force is applied at the contact of the REBCO conductor and spacer. To keep the resultant force zero, the direction of friction force acting on each interface is opposite, but have the same magnitude. The magnitudes of friction forces acting on the upper (f_i^u) and lower boundary (f_i^l) of i^{th} SP are given by:

$$\begin{aligned} f_i^u &= \mu_s \left(P^p + \sum_{j=1}^{i-1} P_j^m \right), \\ f_i^l &= \mu_s \left(P^p + \sum_{j=1}^i P_j^m \right), \end{aligned} \quad (4)$$

where μ_s , P^p , and P_i^m are, respectively, friction coefficient, the pressure applied by preload structure, and axial pressure due to Lorentz force at i^{th} SP. P_i^m is calculated by:

$$P_i^m = \int_{V_i} B_r (J_{tran} + J_{scf}) dV_i, \quad (5)$$

where V_i is the volume of i^{th} SP. Calculated P_i^m values are summarized in Table II.

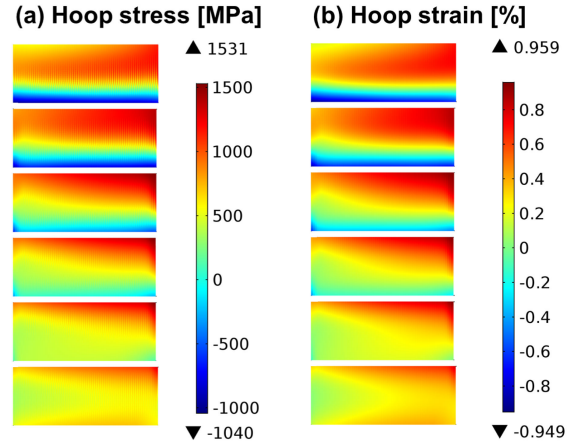


Fig. 4. Hoop stress calculation results in windings of LBC magnet with 0 mm overbanding and 0 friction coefficient: (a) hoop stress; (b) magnetic + bending hoop strain. Since the conductor is wound with the REBCO layer facing radially inward, a negative bending strain is considered. Maximum hoop stress and maximum hoop strain are evaluated to be 1531 MPa and 0.959 % at SP3.

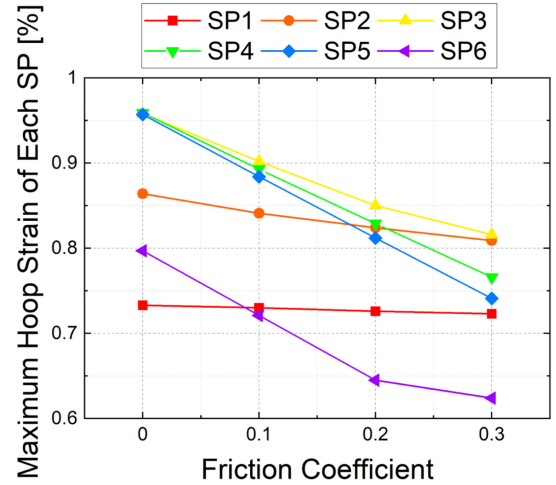


Fig. 5. Maximum hoop strain (magnetic + bending strain) values of each SP coil depending on different friction coefficients. The magnitude of reduction in maximum hoop strain differs by SP, mainly because of the difference in axial pressure induced by Lorentz force.

B. Effect of Friction Force: Reduction of Maximum Stress Without Additional Space

Since the lack of precise measurement on friction coefficient of REBCO conductor in low temperature, sweeping ranges of the friction coefficient between REBCO and spacer are preliminarily set to be from 0 to 0.3 with an interval of 0.1 [26]. Overband structure is neglected. Calculation results of maximum hoop strain (magnetic + bending strain) in each SP depending on different friction coefficient values are presented in Fig. 5. As larger the friction coefficient, the smaller maximum hoop strain is generated within the winding. The effect of the friction coefficient is differed by each SP: as stronger the axial pressure is, the more the friction force tends to influence maximum hoop strain values. Therefore, the SP which experiences maximum hoop strain may be changed depending on the friction coefficient and the coil structure.

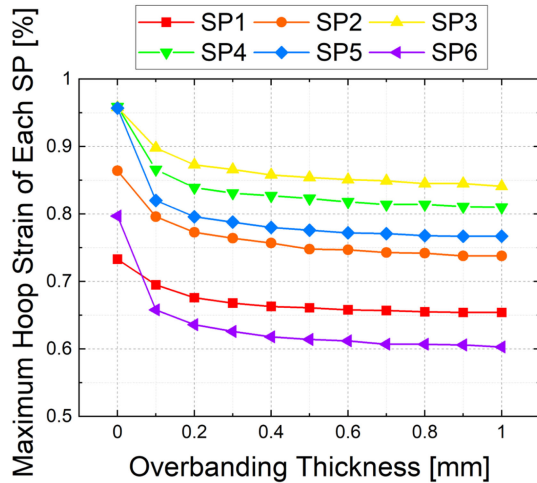


Fig. 6. Maximum hoop strain (magnetic + bending strain) calculation results of each SP depending on overbanding thickness. The effect of overbanding is saturated as the overbanding becomes thicker.

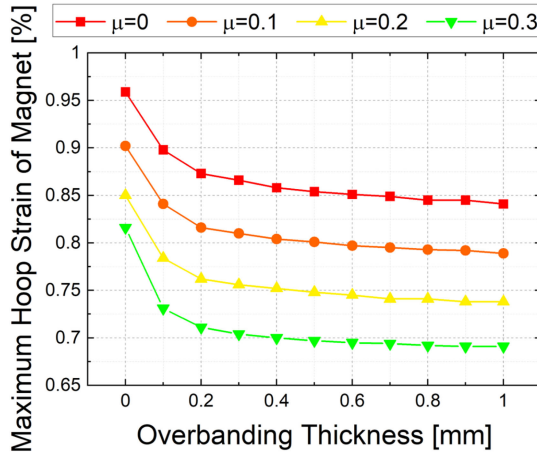


Fig. 7. Maximum hoop strain (magnetic + bending strain) calculation results of the magnet according to the sweep of both friction coefficient and overbanding thickness. Sweeping ranges of friction coefficient and overbanding thickness are, respectively, 0 to 0.3 by 0.1, and 0 mm to 1 mm by 0.1 mm.

C. Effect of Overbanding: Saturation of Maximum Hoop Stress With a Certain Thickness

The thickness of overbanding is swept in the ranges of 0 mm to 1 mm by an interval of 0.1 mm. Bulk stainless steel overband structure is assumed, and friction is neglected for this simulation. Fig. 6 shows comparison results of maximum hoop strain values depending on the thickness of overbanding. Reduction in maximum hoop strain values with increased overbanding thickness is dominant when they are thin (<0.5 mm), but the maximum hoop strain values tend to be saturated with a thicker overbanding.

D. Summary: 0.268% Reduction in Hoop Strain With μ_s of 0.3, and Overbanding of 1 Mm

Fig. 7 shows maximum hoop strains in the winding depending on both sweeping parameters of friction coefficient and overbanding thickness. Ranges of sweeping parameters are 0 to 0.3 by 0.1, and 0 mm to 1 mm by 0.1 mm, respectively for, friction

coefficient and overbanding thickness. Without the help of both constraints, maximum hoop strain is evaluated to be 0.959%, while maximum hoop strain can be reduced by < 0.7% with a friction coefficient of 0.3, and 1 mm thickness overbanding.

IV. DISCUSSION

So far various numerical simulations and experimental studies have been performed to understand screening current stress behavior of NI magnets [25]–[30]. In the context of those studies, our study confirmed that the maximum hoop stress value can be reduced by taking into account the frictional force and overbanding structure. Still, our simulation results overestimate the maximum hoop stress of the magnet like some of those relevant studies. Since the main source of the magnetic stress is non-uniform current density distribution, there exists a possibility that the non-uniform current distribution in the winding is different from that calculated by the current index model. To best of our knowledge, taking into account potential sources such as, but not limited to, local I_c degradation of the conductor, splice resistance, or magnetic field dependence of index value may be a crucial factor that affects current density distributions in the magnet [22], [31]–[34].

V. CONCLUSION

In this study, we investigated the effect of friction force and overbanding structure on screening current induced stress using parameter sweep method. By using the H -formulation together with the 2D edge element and domain homogenization method, non-uniform current density distributions of our target analysis model, Little Big Coil (LBC), were calculated. From the calculated current density, we constructed a mechanical model that enables to express axial interactions between adjacent single pancake (SP) by modeling every SP coils. The friction acts in between the SP and G10 spacer with the direction of limiting radial displacement, while frictionless contact is assumed for the radial turn-to-turn contact of NI windings. Finally, we reached the following conclusions by our parameter sweep results.

- Commonly, several ultra high field magnets are designed, and constructed with overbanding thickness of > 1 mm [6], [35]. As our results show that the effect of friction is dominant when overbanding is thicker than 0.5 mm, friction may play an important role in reducing peak magnetic stress.
- The larger the axial pressure and the friction coefficient, the larger the reduction in maximum hoop strain due to friction force.
- As expected, overbanding reduced peak hoop strain of the magnet, but its effect gradually diminishes with thicker overbanding.
- Presence of both friction and overbanding effectively reduce peak hoop strain level. Our results imply 0.268% of strain reduction in LBC magnet with a help of 1 mm overbanding and friction coefficient of 0.3.

REFERENCES

- [1] S. Hahn *et al.*, "45.5-tesla direct-current magnetic field generated with a high-temperature superconducting magnet," *Nature*, vol. 570, pp. 496–499, 2019.
- [2] G. Nishijima *et al.*, "Successful upgrading of 920-MHz NMR superconducting magnet to 1020 MHz using Bi-2223 innermost coil," *IEEE Trans. Appl. Supercond.*, vol. 26, no. 3, Feb. 2016, Art. no. 4303007.
- [3] S. Yoon, J. Kim, K. Cheon, H. Lee, S. Hahn, and S.-H. Moon, "26 T, 35 mm all-GdBa₂Cu₃O_{7-x} multi-width no-insulation superconducting magnet," *Supercond. Sci. Technol.*, vol. 29, no. 4, 2016, Art. no. 04LT04.
- [4] J. Liu *et al.*, "World record 32.35 tesla direct-current magnetic field generated with an all-superconducting magnet," *Supercond. Sci. Technol.*, vol. 33, no. 3, 2020, Art. no. 03LT01.
- [5] K. L. Kim *et al.*, "400-MHz/60-mm All-REBCO nuclear magnetic resonance magnet: Magnet design," *IEEE Trans. Appl. Supercond.*, vol. 26, no. 4, Jun. 2015, Art. no. 4302604.
- [6] P. C. Michael *et al.*, "Assembly and test of a 3-nested-coil 800-MHz REBCO insert (H800) for the MIT 1.3 GHz LTS/HTS NMR magnet," *IEEE Trans. Appl. Supercond.*, vol. 29, no. 5, Aug. 2019, Art. no. 4300706.
- [7] P. Fazilleau, X. Chaud, F. Debray, T. L  crevisse, and J.-B. Song, "38 mm diameter cold bore metal-as-insulation HTS insert reached 32.5 T in a background magnetic field generated by resistive magnet," *Cryogenics*, vol. 106, 2020, Art. no. 103053.
- [8] Y. Iwasa and S. Hahn, "First-cut design of an all-superconducting 100-T direct current magnet," *Appl. Phys. Lett.*, vol. 103, no. 25, 2013, Art. no. 253507.
- [9] W. D. Markiewicz *et al.*, "Design of a superconducting 32 T magnet with REBCO high field coils," *IEEE Trans. Appl. Supercond.*, vol. 22, no. 3, Jun. 2011, Art. no. 4300704.
- [10] J. Kim *et al.*, "Design, construction, and operation of an 18 T, 70 mm no-insulation (RE) Ba₂Cu₃O_{7-x} magnet for an axion haloscope experiment," *Rev. Sci. Instrum.*, vol. 91, no. 2, 2020, Art. no. 023314.
- [11] S. Hahn, D. K. Park, J. Bascunan, and Y. Iwasa, "HTS pancake coils without turn-to-turn insulation," *IEEE Trans. Appl. Supercond.*, vol. 21, no. 3, pp. 1592–1595, Jun. 2011.
- [12] J.-B. Song, S. Hahn, T. L  crevisse, J. Voccio, J. Bascu  n, and Y. Iwasa, "Over-current quench test and self-protecting behavior of a 7 T/78 mm multi-width no-insulation REBCO magnet at 4.2 K," *Supercond. Sci. Technol.*, vol. 28, no. 11, 2015, Art. no. 114001.
- [13] Y. Wang, W. K. Chan, and J. Schwartz, "Self-protection mechanisms in no-insulation (RE) Ba₂Cu₃O_x high temperature superconductor pancake coils," *Supercond. Sci. Technol.*, vol. 29, no. 4, 2016, Art. no. 045007.
- [14] K. Kim *et al.*, "Quench behavior of a no-insulation coil wound with stainless steel cladding REBCO tape at 4.2 K," *Supercond. Sci. Technol.*, vol. 30, no. 7, 2017, Art. no. 075001.
- [15] S. Hahn *et al.*, "No-insulation multi-width winding technique for high temperature superconducting magnet," *Appl. Phys. Lett.*, vol. 103, no. 17, 2013, Art. no. 173511.
- [16] X. Hu *et al.*, "Analyses of the plastic deformation of coated conductors deconstructed from ultra-high field test coils," *Supercond. Sci. Technol.*, vol. 33, no. 9, 2020, Art. no. 095012.
- [17] R. Brambilla, F. Grilli, and L. Martini, "Development of an edge-element model for AC loss computation of high-temperature superconductors," *Supercond. Sci. Technol.*, vol. 20, no. 1, pp. 16–24, 2006.
- [18] V. M. Zermeno, A. B. Abrahamsen, N. Mijatovic, B. B. Jensen, and M. P. S  rensen, "Calculation of alternating current losses in stacks and coils made of second generation high temperature superconducting tapes for large scale applications," *J. Appl. Phys.*, vol. 114, no. 17, 2013, Art. no. 173901.
- [19] J. Bang *et al.*, "Field measurement and analysis of a 3 T 66 mm no-insulation HTS NMR magnet with screening current and manufacturing uncertainty considered," *IEEE. Trans. Appl. Supercond.*, vol. 29, no. 5, Feb. 2019, Art. no. 4601305.
- [20] J. Rhyner, "Magnetic properties and AC-losses of superconductors with power law current-voltage characteristics," *Phys. C*, vol. 212, pp. 292–300, 1993.
- [21] D. Hilton, A. Gavrilin, and U. Trociewitz, "Practical fit functions for transport critical current versus field magnitude and angle data from (RE)BCO coated conductors at fixed low temperatures and in high magnetic fields," *Supercond. Sci. Technol.*, vol. 28, no. 7, 2015, Art. no. 074002.
- [22] C. Zhou, K. Yagotintsev, P. Gao, T. Haugan, D. van Der Laan, and A. Nijhuis, "Critical current of various REBCO tapes under uniaxial strain," *IEEE. Trans. Appl. Supercond.*, vol. 26, no. 4, Jun. 2016, Art. no. 8401304.
- [23] D. Peric and D. Owen, "Computational model for 3-D contact problems with friction based on the penalty method," *Internat. J. Numer. Methods. Engrg.*, vol. 35, no. 6, pp. 1289–1309, 1992.
- [24] P. Wriggers and G. Zavarise, *Computational Contact Mechanics*. Hoboken, NJ, USA: Wiley, 2004.
- [25] J. Xia, H. Bai, H. Yong, H. W. Weijers, T. A. Painter, and M. D. Bird, "Stress and strain analysis of a REBCO high field coil based on the distribution of shielding current," *Supercond. Sci. Technol.*, vol. 32, no. 9, 2019, Art. no. 095005.
- [26] Y. Li *et al.*, "Magnetization and screening current in an 800 MHz (18.8 t) REBCO nuclear magnetic resonance insert magnet: Experimental results and numerical analysis," *Supercond. Sci. Technol.*, vol. 32, no. 10, 2019, Art. no. 105007.
- [27] Y. Li *et al.*, "Screening-current-Induced strain gradient on RE-BCO conductor: An experimental and analytical study with small coils wound with monofilament and striated multifilament REBCO tapes," *IEEE. Trans. Appl. Supercond.*, vol. 30, no. 4, Jun. 2020, Art. no. 4702305.
- [28] S. Takahashi *et al.*, "Hoop stress modification, stress hysteresis and degradation of a REBCO coil due to the screening current under external magnetic field cycling," *IEEE. Trans. Appl. Supercond.*, vol. 30, no. 4, Jun. 2020, Art. no. 4602607.
- [29] Y. Yan, C. Xin, M. Guan, H. Liu, Y. Tan, T. Qu, "Screening current effect on the stress and strain distribution in REBCO high-field magnets: Experimental verification and numerical analysis," *Supercond. Sci. Technol.*, vol. 33, no. 5, 2020, Art. no. 05LT02.
- [30] D. J. Kolb-Bond *et al.*, "Computing strains due to screening currents in REBCO magnets," *IEEE. Trans. Appl. Supercond.*, vol. 30, no. 4, Jun. 2020, Art. no. 4602805.
- [31] C. Barth, G. Mondonico, and C. Senatore, "Electro-mechanical properties of REBCO coated conductors from various industrial manufacturers at 77 k., self-field and 4.2 k, 19 T," *Supercond. Sci. Technol.*, vol. 28, no. 4, 2015, Art. no. 045011.
- [32] V. Zermeno, P. Kr  ger, M. Takayasu, and F. Grilli, "Modeling and simulation of termination resistances in superconducting cables," *Supercond. Sci. Technol.*, vol. 27, no. 12, 2014, Art. no. 124013.
- [33] T. Benkel, Y. Miyoshi, X. Chaud, A. Badel, and P. Tixador, "REBCO tape performance under high magnetic field," *Eur. Phys. J. Appl. Phys.*, vol. 79, no. 3, 2017, Art. no. 30601.
- [34] X. Zhang *et al.*, "Study of critical current and n-values of 2 G HTS tapes: Their magnetic field-angular dependence," *J. Supercond. Novel Mag.*, vol. 31, no. 12, pp. 3847–3854, 2018.
- [35] M. Guan *et al.*, "A parametric study on overband radial build for a REBCO 800-MHz insert of a 1.3-GHz LTS/HTS NMR magnet," *IEEE. Trans. Appl. Supercond.*, vol. 26, no. 4, Jun. 2016, Art. no. 4301205.